Fuel 196 (2017) 154–168

Contents lists available at ScienceDirect

Fuel

journal homepage: www.elsevier.com/locate/fuel

Full Length Article

Effect of ethanol blending on particulate formation from premixed combustion in spark-ignition engines

Stephen Sakai [a,*], David Rothamer [b]

[a] University of Wisconsin-Madison, 1500 Engineering Dr, ERB 140, Madison, WI 53706, USA
[b] University of Wisconsin-Madison, 1500 Engineering Dr, ERB 127, Madison, WI 53706, USA

ARTICLE INFO

Article history:
Received 25 October 2016
Received in revised form 11 January 2017
Accepted 13 January 2017
Available online 4 February 2017

Keywords:
Gasoline
Ethanol
Particulate
Soot
Size distribution
Combustion
Premixed

ABSTRACT

Particulate formation due to combustion of a wide range of ethanol-gasoline blends were investigated in an internal combustion engine. The engine used for this study is a single-cylinder research engine, the architecture of which is representative of a modern spark ignited direct injected (SIDI) engine. Instead of direct injection, the engine was fueled using a premixed prevaporized (PMPV) mode, which supplied the fuel to the engine in a well-mixed, gas-phase air-fuel mixture in order to isolate physical effects of the fuel. This created a completely homogenous air-fuel mixture with no pockets of significantly differing equivalence ratio, liquid fuel droplets, or wetted surfaces, ensuring that particulate formation was due to homogenous, gas-phase combustion. The engine was operated at a fixed load and phasing so that the effects of varying equivalence ratio and ethanol content could be examined. The results in this work show that the addition of ethanol results in a consistent decrease in engine-out particulate proportional to ethanol content. Moreover, the critical equivalence ratio, the equivalence ratio at which significant sooting begins, increases in a linear fashion with ethanol addition. It was also shown that the shape of the particulate size distribution (PSD) is affected by ethanol content, with increased ethanol leading to more nucleation-mode dominated distributions.

1. Introduction

Renewable energy standards in the US have positioned ethanol addition to gasoline squarely into the long-term view. Currently, gasoline in the United States contains up to 10% ethanol by volume (E10); however, the United States Environmental Protection Agency (EPA) has already begun allowing E15 to be sold to consumers [1] and this allowance has opened the door for future increases. With stricter particulate matter (PM) regulation in Europe and the US putting more focus on PM emissions from spark-ignited (SI) engines, and increasing ethanol content in gasoline, it is important to understand how ethanol blending influences the sooting tendency of gasoline in a comprehensive way.

Engine-out PM emissions from ethanol-blended gasoline are still not nearly as well understood as those for diesel or gasoline. Most gasoline-ethanol PM research in the literature has focused on low ethanol blend percentages (<20 vol.%). Laboratory flame studies have concentrated on the formation of soot precursors. Ethanol was shown to reduce aromatic species in an ethylene premixed flame for concentrations up to 10% by mass [2–5]. However, in non-premixed ethylene flames it was found that ethanol addition increased soot production for the same concentrations [6,7]. Salamanca et al. found similar increases in soot for low concentration ethanol blends with ethylene in a counterflow diffusion flame but saw a decrease when the ethanol content exceeded 20% by mass [8]. Similar results were found with higher hydrocarbons. Rubino et al. found increased benzene in a counterflow diffusion propane flame with 10% ethanol addition by volume, followed by a decrease when ethanol concentration was increased to 15% [9]. Experiments with toluene, isooctane, *n*-heptane, and gasoline showed similar trends [10–14].

The differences in laboratory flame results show that the effect of small concentrations of ethanol will depend on the mode of combustion: premixed or diffusion controlled burning. Conversely, larger fractions of ethanol consistently show decreases in soot and soot precursors. This has been attributed to both the dilution of a more sooting fuel with less sooting ethanol [13,15,16], as well as the chemical effect of the oxygen in the fuel reducing the available pathways for soot formation [3,4,17].

Engine studies in the literature which include ethanol generally have also focused on low ethanol blend percentages. Much like flame studies, there is not always a consistent trend. Some studies

* Corresponding author.
E-mail addresses: ssakai@wisc.edu (S. Sakai), rothamer@engr.wisc.edu (D. Rothamer).

http://dx.doi.org/10.1016/j.fuel.2017.01.070
0016-2361/

showed little to no sensitivity to ethanol content up to 10% by volume, indicating that engine operating conditions played a more critical role in reducing engine PM [18–20]. Price et al. showed little change in PM for ethanol concentrations up to 30% but indicated a large reduction for E85 [21]. Other work showed a consistent decrease in PM with ethanol content [22–24]. In contrast, Catapano et al. and Di Iorio and coworkers indicated that E50 and E85 made more particulate than neat gasoline [25,26]. Nearly all studies cite engine operation as a significant factor in the results due to the operating condition's effect on parameters such as air-fuel mixture preparation, fuel vaporization, and wetting of surfaces.

The purpose of this study is to examine the effect of ethanol addition to gasoline on particulate formation in a spark-ignition engine while minimizing the effects of mixture preparation and engine operating condition. To accomplish this, a previously reported operation method was utilized in which fuel was introduced to the intake air stream far upstream of the engine [27]. This method, called premixed prevaporized (PMPV) operation, ensures that the fuel is completely premixed and prevaporized before reaching the engine. Changes in fuel physical properties due to ethanol addition can directly affect mixture preparation. By premixing and prevaporizing the fuel in advance, the majority of physical effects of the fuel can be removed. This allows for an air-fuel mixture which is completely homogenous, eliminating any pockets of significantly differing equivalence ratio, liquid fuel droplets, or wetted surfaces which could easily occur under direct-injection operation. Also removed is the effect of evaporative cooling from the fuel which can create different in-cylinder conditions. Thus, any soot formed in this operating mode can only be attributed to the combustion of homogenously-mixed gas-phase fuel components under comparable in-cylinder conditions.

2. Experimental setup

2.1. Engine

The engine used for these experiment is a single-cylinder engine which has been configured to be representative of a modern spark-ignited direct injection (SIDI) engine. The cylinder head features a 4-valve pent-roof combustion chamber with a centrally mounted spark plug and a side-mounted fuel injector. Table 1 lists the specifications for the engine. It should be noted that all engine timings are listed with 0 crank angle degree (CAD) referenced to top dead center (TDC) of the compression stroke, times before TDC are negative and times after TDC are positive. In-cylinder pressure was measured using a high-speed piezo-electric pressure transducer (Kistler 6125C). An average of 50 cycles of measured pressure was used to set the operating condition based on gross indicated mean effective pressure ($IMEP_g$) and location of 50% cumulative heat release (CA50). Pressure data was acquired for 500 cycles and averaged. A MATLAB post-processor was used to calculate cumulative heat release, heat release rate, and mass averaged in-cylinder temperature.

For this work, the in-cylinder fuel injector was replaced with a plug and was moved to a premixing chamber upstream of the intake surge tank. As mentioned before, under PMPV operation, fuel is injected far upstream of the intake such that it is premixed and vaporized by the time it enters the engine. Complete vaporization is verified by shining a laser through an observation window just upstream of the engine. Laser light is scattered by any droplets present, indicating the presence of liquid fuel. This method isolates liquid fuel and spray effects from the particulate formation process, enabling the investigation of fuel chemistry impacts on PM, specifically the effect of the fuel-bound oxygen for ethanol-gasoline blends. For all test conditions, the engine was held at constant speed, load, and combustion phasing as listed in Table 2.

Table 1
Engine geometric parameters.

Parameter	Value	Unit
Bore	85.96	mm
Stroke	94.6	mm
Displacement	549	cm^3
Compression ratio	11.97	
Connecting rod length	152.4	mm
Intake valve open	+350	CAD
Intake valve close	−140	CAD
Exhaust valve open	+150	CAD
Exhaust valve close	−355	CAD
Intake/exhaust valve lift	9.9	mm

Table 2
Nominal engine operating parameters corresponding to EEE $\Phi = 0.98$ baseline condition.

Parameter	Value	Unit
Engine speed	2100	RPM
$IMEP_g$	334	kPa
CA50	+8.0	CAD
Spark timing	−25	CAD
Intake pressure	35	kPa
Exhaust pressure	101.5	kPa
Intake temperature	60	°C
Exhaust sample temperature	250	°C
Fuel pressure	9	MPa
Indicated power	3.2	kW

2.2. Particulate sampling system

Engine out particle size distributions (PSDs) were measured using a particulate sampling system composed of a dilution system (Dekati FPS 4000) and a scanning mobility particle sizer (SMPS). The SMPS utilizes an electrostatic classifier (EC, TSI model 3080), a differential mobility analyzer (LDMA, TSI model 3081), and a condensation particle counter (CPC, TSI model 3010). A diagram of the exhaust sampling system is shown in Fig. 1. Exhaust is sampled at a location downstream of the exhaust surge tank. The dilution

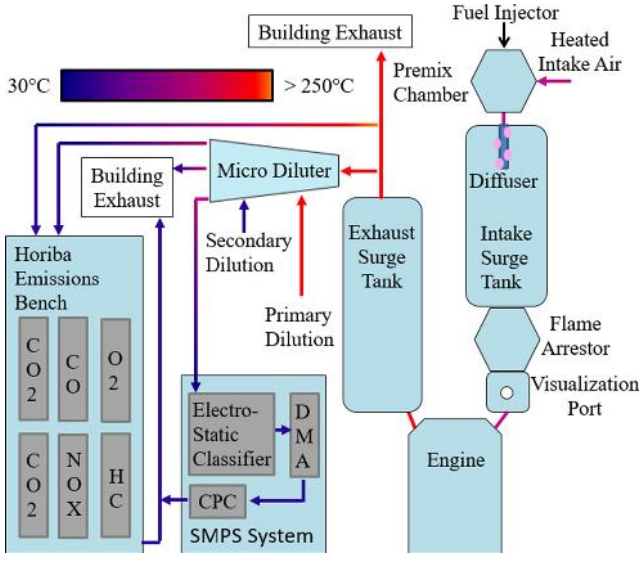

Fig. 1. Experimental setup schematic showing the exhaust sampling system.

process is performed in two stages. The first uses filtered air heated to 400 °C to maintain near isothermal dilution at the sample temperature, which is approximately 250 °C, this is then followed by a second stage dilution with filtered air at ambient temperature. The total dilution ratio for these experiments was maintained above 30:1. After dilution, the EC and LDMA classify particles according to mobility diameter (d_m) in a range from 7 to 300 nm from the diluted exhaust stream and sends them to the counter. A Horiba 6-gas emissions bench was used to measure undiluted gaseous emissions: hydrocarbons (HC), carbon monoxide (CO), carbon dioxide (CO_2), nitrogen oxides (NO_x), oxygen (O_2), as well as diluted CO_2 which was used to determine the real-time dilution ratio.

To measure particle mass, a centrifugal particle mass analyzer (CPMA, Cambustion) was used. The mass was then correlated to mobility diameter by measuring in combination with the SMPS. Particles were selected based on mass by the CPMA before being sent to the SMPS for mobility diameter classification. This method is similar to the that which was performed in [28].

Table 3
Properties of gasoline and ethanol fuel.

Property	EEE	E100[a]	Unit
RON	97.2	108.6	
Lower heating value	42.8	26.9	MJ/kg
Density @ 293 K	0.744	0.789	kg/L
Boiling point	T10 = 326 T50 = 377 T90 = 434	351	K
Heat of vaporization @ 298 K	349	931.1	kJ/kg
Reid vapor pressure	61.3	15.9	kPa
Aromatics	28	0	%
Olefins	2	0	%
Saturates	70	0	%
Hydrogen/carbon ratio	1.845	3	
Oxygen/carbon ratio	0	0.5	
Stoichiometric Air-fuel ratio	14.6	8.97	

[a] Values given are for neat ethanol. Ethanol used in this study contained 3.27% denaturant by volume.

2.3. Fuels

In this study, 2 base fuels were used: Tier II EEE gasoline and denatured ethanol (E100, 3.27% denaturant), both supplied by Haltermann Products. These were splash blended to create 10, 20, 30, 40, and 50 vol.% blends of ethanol with gasoline (E10, E20, E30, E40, and E50). The properties of the base fuels are shown in Table 3. Maximum ethanol blend percentage was limited to 50 vol.% because higher ethanol blends did not generate measurable particulate above the baseline level for the highest equivalence ratios that could be tested.

3. Results

3.1. Matching of experimental conditions

For this work, the experimental results consist of equivalence ratio sweeps at a fixed load (constant gross indicated mean effective pressure, $IMEP_g$), fixed combustion phasing (constant CA50), and fixed engine speed for each fuel. The goal is to isolate the equivalence ratio change as the primary variable when performing the experiments, such that the chemical sooting tendency of each fuel blend can be assessed. Fig. 2(a) shows pressure traces for selected EEE cases over a range of equivalence ratios. The trace for each equivalence ratio represents the mean of 500 engine cycles. The peak pressures are all within ~5% of each other (~1 bar) and the pressures at all other crank angles (CA) are also within this tolerance. The pressure traces match well due to the matching of load and CA50. Fig. 2(b) also shows the average bulk temperature traces for the same conditions. It can be seen that the bulk temperature decreases with enrichment. This decrease is expected as the added in-cylinder mass for rich equivalence ratios acts as a diluent. While there is a noticeable change in temperature over the entire equivalence ratio range, as will be shown, the difference in temperature over the equivalence ratio range where the sooting threshold is crossed is relatively small. For all fuels, the transition from non-sooting to sooting occurs over an equivalence ratio change of less than 0.05. EEE is shown here but all of the fuels tested followed this trend.

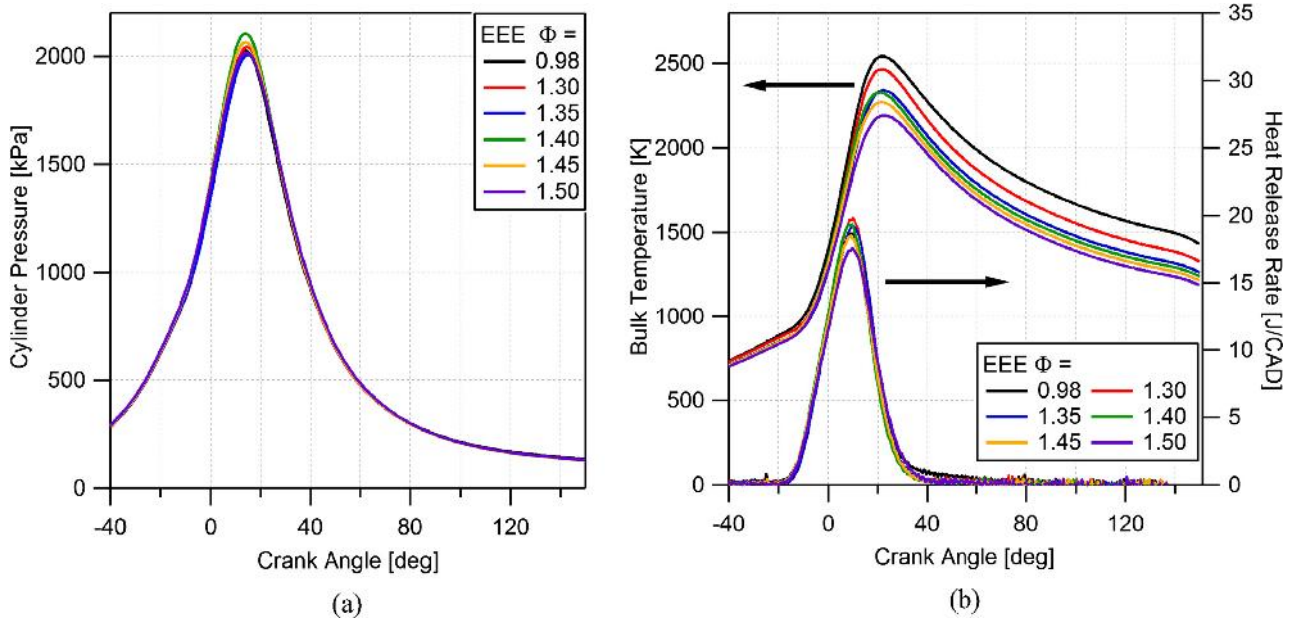

Fig. 2. Sample pressure (a) and temperature (b) traces showing load matched conditions for EEE fuel.

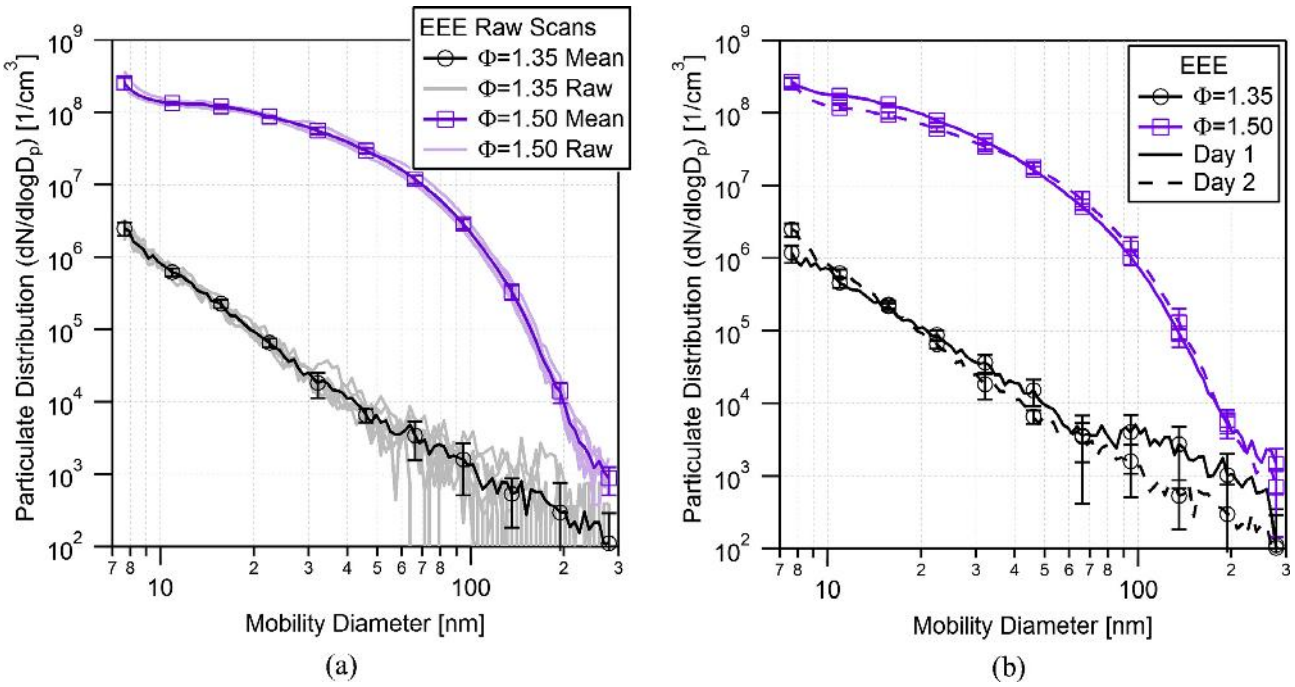

Fig. 3. (a) Raw SMPS scans for selected cases with mean and 95% confidence intervals shown. (b) Day-to-day repeatability for two selected cases with repeated data shown with dashed lines.

3.2. Experimental repeatability

Along with the matching of experimental conditions, care was taken to minimize variables which could impact experimental repeatability. Each data point consists of a minimum of 7 SMPS scans taken while the engine operating conditions are held constant. These scans are then processed to determine a mean and 95% confidence interval for the PSD. Two example data sets are shown in Fig. 3, Fig. 3(a) illustrates typical scan-to-scan variability and Fig. 3(b) typical day-to-day variability seen in these experiments. In Fig. 3(a), the lower equivalence ratio case shown here illustrates the increase in variability as the particulate concentration approaches the detection limit of the instrument. As the concentration increases, this variability reduces as can be seen in the higher equivalence ratio case. Day-to-day variability, shown in (b) of Fig. 3, for the data is similar. Here, two data sets taken weeks apart are shown. There is some variation in the PSD, but largely the shape and magnitude are repeated. Again, in the areas where the instrument is near the detection limit, the variability is increased.

3.3. Confirmation of non-fuel baseline particulate level

Previous work by Hageman et al. [27] has shown that, for this engine at a fixed operating condition (i.e., fixed engine load, speed, and CA50), there is a minimum particulate level that is independent of fuel type. The particulate was hypothesized to be due to non-fuel sources such as engine oil and wear particles. It was found that the particulate remained constant at this minimum level until the equivalence ratio was raised beyond a threshold equivalence ratio. This baseline particulate level was termed the non-fuel baseline (NFB) and the enrichment level at which particulate increased significantly above the NFB was referred to as the critical equivalence ratio (Φ_c).

Fig. 4 shows size distributions for all of the fuels at a near stoichiometric equivalence ratio. Each trace shown is the mean PSD for that case with markers shown at every 10th data point. Error bars shown represent a 95% confidence interval about the mean.

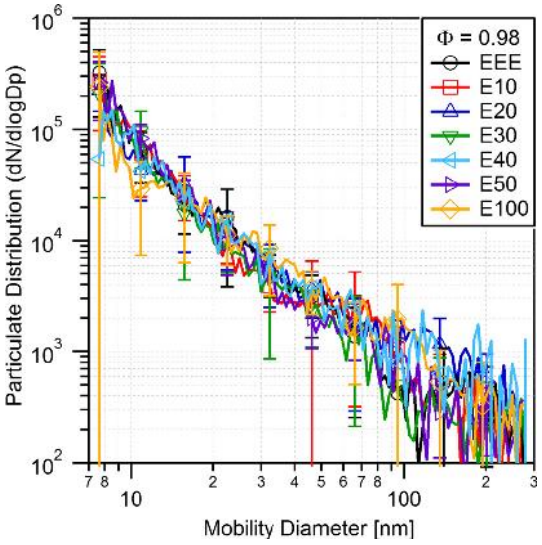

Fig. 4. Particle size distributions for EEE, E100, and all ethanol-gasoline blends tested at the standard operating conditions with $\Phi = 0.98$.

Fig. 4 demonstrates that there is no significant difference between the different fuels under PMPV operation with an equivalence ratio of 0.98. These results agree with the previous results of Hageman et al., with the measured size distributions corresponding to the NFB.

3.4. Effects of enrichment

At near stoichiometric equivalence ratios, all of the tested fuels show the same PSD, which is indicative of the NFB mentioned previously. As the equivalence ratio is increased above stoichiometric, a different behavior is displayed by each fuel. Figs. 5 and 6 show the PSD results for each fuel at different equivalence ratios. For easier visualization, across all of the plots, similar equivalence

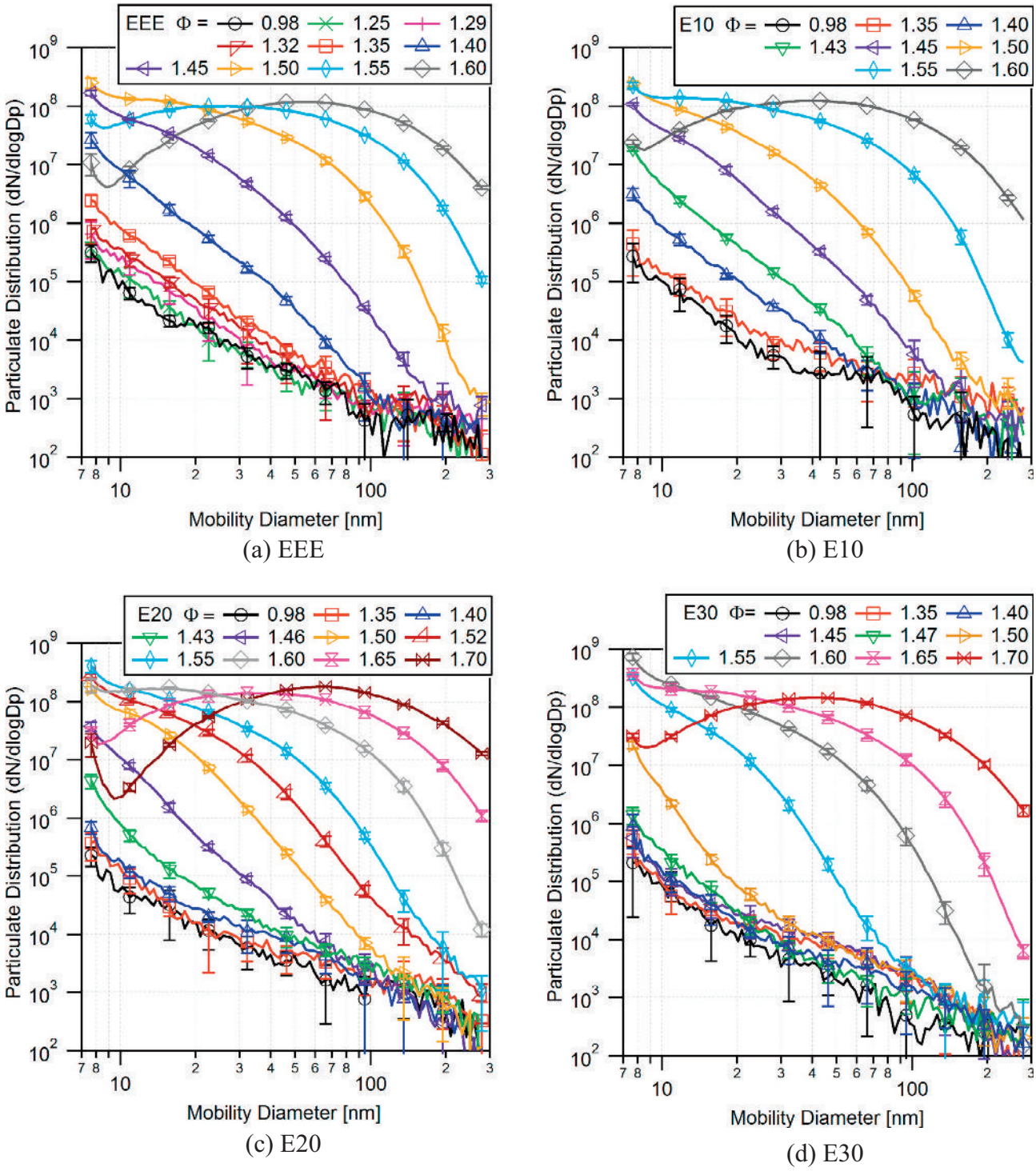

Fig. 5. Particle size distributions for (a) EEE, (b) E10, (c) E20, and (d) E30 tested at various equivalence ratios.

ratios are represented with the same color[1]/symbol and the same y-axis scale range is used in all plots.

As can be seen in Figs. 5 and 6, the equivalence ratio at which each fuel begins to make significant particulate over the NFB increases with ethanol content. EEE begins to show a small increase at $\Phi = 1.35$, followed by larger increases with each equivalence ratio step. Each fuel follows a similar trend, first there is an increase in nucleation-mode particles (where nucleation-mode particles for this work are defined as those with mobility diameter (d_m) < 30 nm), as the number of particles increases the diameter where the distribution stops deviating from the NFB increases. At sufficiently high equivalence ratios, an increase in particle number relative to the NFB is seen at all mobility diameters within the instrument measurement range. At high equivalence ratios, the distributions shifts from being dominated by nucleation-mode particles to being dominated by agglomerate-mode (synonymous with accumulation-mode) particles with $d_m > 30$ nm.

[1] For interpretation of color in all figures, the reader is referred to the web version of this article.

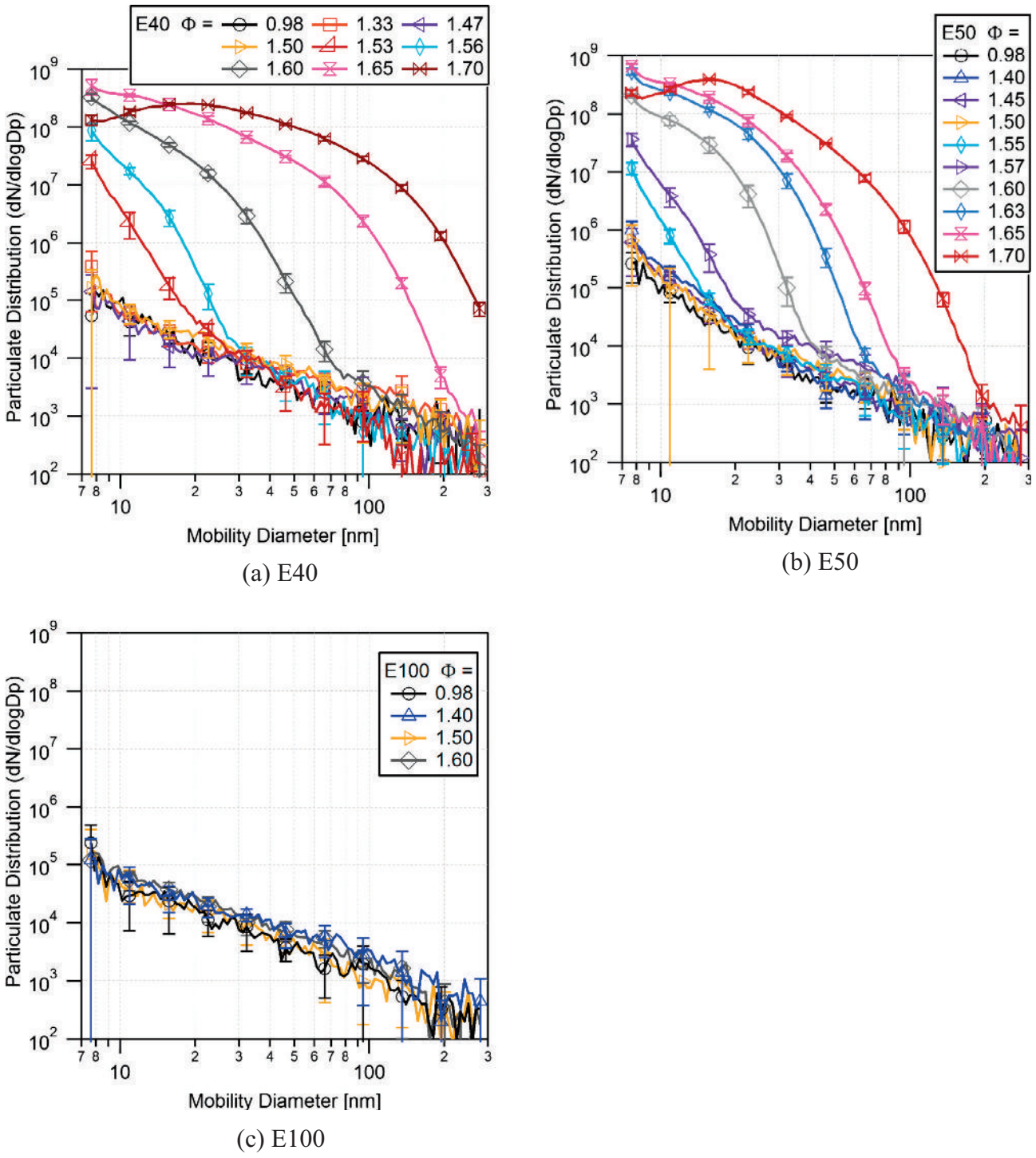

Fig. 6. Particle size distributions for (a) E40, (b) E50, and (c) E100 tested at various equivalence ratios.

However, as the ethanol content increases, the behavior changes slightly. For lower level ethanol blends, EEE through E30, as the equivalence ratio increases the PSD shifts from nucleation-mode dominated at low to middle equivalence ratios to agglomeration-mode dominated at the highest equivalence ratios. As ethanol content in the fuel is increased, the magnitude of this shift lessens; for E20 and E30 this shift happens at much higher Φ. E40 and E50 show no increase in particulate until Φ > 1.50 and, while the level of larger particles increases at the extreme equivalence ratios, a shift to larger particles is not as pronounced as the lower fuel blends. In particular, there appears to be a distinct change in the distribution shape for E40 and E50 with a distinct kink in the distribution appearing around 20 nm as compared to the well round distribution seen for lower-level blends. The E100 results, shown in Fig. 6(c), show no change in particulate levels from the NFB for equivalence ratios up to 1.60. This result for E100 agrees with previous findings from Hageman et al. [27].

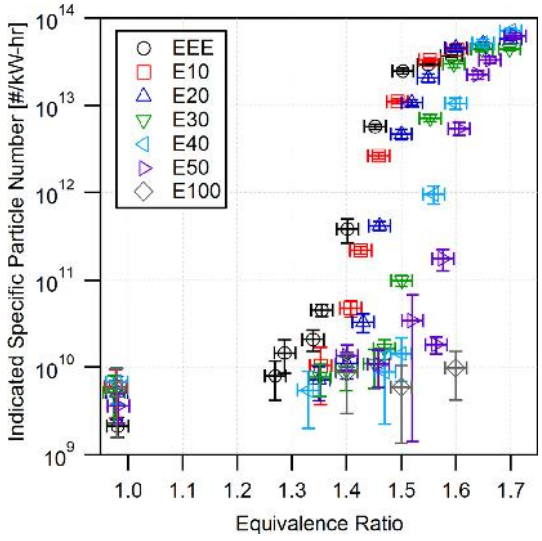

Fig. 7. Indicated specific particle number for each fuel as a function of equivalence ratio.

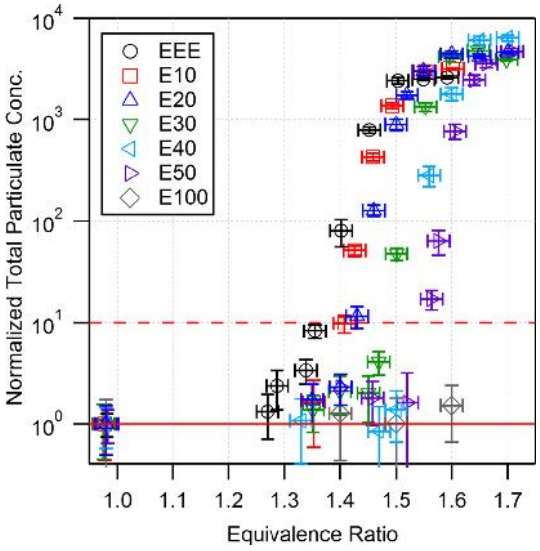

Fig. 8. Total particle concentrations normalized to NFB shown with 10× threshold line.

3.5. Determination of Φ_c

The particulate results were also examined to compare the total number of particles produced by each fuel. The PSDs for each case were integrated to produce a total concentration, the results of which are shown in Fig. 7 on an indicated specific basis. Indicated specific particle number (ISPN) relates the engine out particulate to the amount of work performed by the engine. This metric is used as it allows more direct comparison of particulate results between different engine platforms. The total concentration is related to the ISPN by

$$ISPN = \frac{N\dot{m}}{\rho \dot{W}} \tag{1}$$

$$\rho = \frac{P_{SMPS}}{R_{exh} T_{SMPS}} \tag{2}$$

where N is the total number concentration, $\dot{m}$ is the total mass flow rate out of the engine, and $\dot{W}$ is the work performed by the engine and ρ is the density of the exhaust sample. The exhaust sample density is calculated using the ideal gas law, where pressure and temperature are taken to be the conditions at the SMPS inlet, and the gas constant is determined using emissions measurements to calculate an average molecular weight of the exhaust sample.

Upon initial inspection, it can be seen that all of the fuels in Fig. 7 have similar ISPN at a stoichiometric equivalence ratio due to all fuels being at the NFB. Differences in the ISPN at this condition are representative of the day-to-day repeatability of the measurements. As Φ increases, each fuel shows an increase in total number at an equivalence ratio that is unique for each fuel blend. This equivalence ratio is the fuel's critical equivalence ratio, Φ_c. Once Φ_c for a fuel has been reached, the particle number increases exponentially until it begins to asymptote at higher equivalence ratios. This asymptotic behavior is believed to be due to the rate of particle agglomeration approaching the rate of particle inception. Interestingly, all of the fuels appear to approach a similar maximum total particle number. Higher ethanol blends, E40 and E50, appear to have slightly higher peak values due to the higher number of nucleation-mode particles and reduction in agglomeration-mode particles.

To determine the critical equivalence ratio, the total concentrations are normalized by the NFB concentration. For this study, Φ_c is considered to be reached when the normalized concentration reaches a threshold set at 10 times the level of the NFB. The normalized concentrations and the 10× threshold are both shown in Fig. 8. To determine Φ_c, an exponential curve fit was applied to the area where the normalized concentration rose exponentially; the location where the fit crosses the 10× threshold was then located. The use of a 10× threshold instead of extrapolation back to the NFB, also used by Hageman et al. [27], is chosen here due to the ease of application and the similarity of the values to those obtained using extrapolation of the curves to the NFB. The critical equivalence ratios determined using the 10× threshold method are given in Table 4. The Φ_c determined using the 10× threshold match the approximate values expected based on the PSD results shown previously in Figs. 5 and 6. Gasoline (EEE) has the lowest Φ_c followed by a steady increase in Φ_c with increasing ethanol content.

The particle number increase in the region near the critical equivalence ratio is very steep. This makes it difficult experimentally to obtain more than a few points in this region. Alternatively, the data can also be examined on a total mass basis using a mass-mobility relationship to determine particle mass. Previous work performed with researchers from Pacific Northwest National Laboratories characterized the relationship between mobility diameter and particle mass for particulate generated by this engine [29]. Data from that study for EEE and ethanol-EEE blends is shown in Fig. 9. Mass measurements were performed using a centrifugal particle mass analyzer (CPMA, Cambustion), while mobility diameter was determined using the SMPS.

To ascribe a mass to particles of different mobility diameter, a two part fit was employed. For particles below 30 nm, it was assumed that the particles were spherical with a density of

Table 4
Critical equivalence ratios by total number and total mass methods.

Fuel	Number Φ_c	Mass Φ_c
EEE	1.35 ± 0.02	1.38 ± 0.02
E10	1.39 ± 0.02	1.42 ± 0.02
E20	1.43 ± 0.02	1.46 ± 0.02
E30	1.47 ± 0.02	1.50 ± 0.02
E40	1.51 ± 0.02	1.54 ± 0.02
E50	1.55 ± 0.02	1.58 ± 0.02

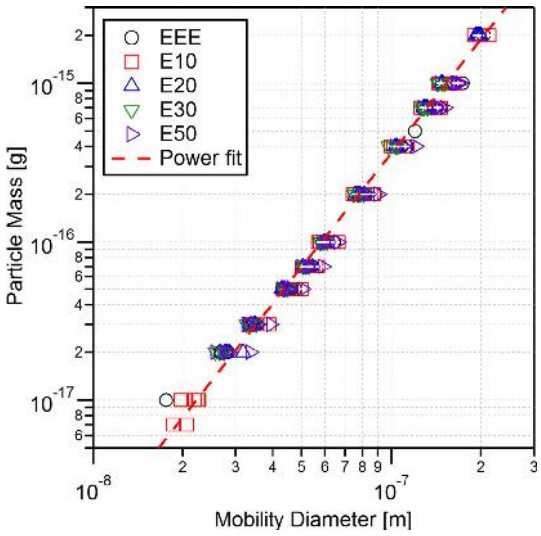

Fig. 9. Particle mass-mobility relation derived from simultaneous particle mass and mobility diameter measurements.

2 g/cm^3. Above 30 nm, the data shown in Fig. 9 was curve fit using a least squares regression to the form

$$m = Cd_m^{D_{fm}} \tag{3}$$

where C is the proportionality coefficient and D_{fm} is the mass-mobility fractal dimension. From the fitting process, the coefficient $C = 21.26$ g/m$^{2.395}$ and the mass-mobility fractal dimension $D_{fm} = 2.395$.

Using the mass-mobility relationship and converting the PSD to a particle mass distribution, the total particle mass can be obtained and a similar normalization procedure, as was used for the total number, can be applied. The result is shown in Fig. 10. Compared to total concentration, total mass does not reach a maximum value. Instead, mass continues to increase exponentially. For higher ethanol blend fractions, however, there still appears to be a slightly decreasing trend in the rate of mass increase at higher equivalence ratios. As was done for the total concentration, an exponential curve was fit to the total mass data for each fuel in the region near Φ_c, and the location of Φ_c was found using the 10× NFB threshold. These results are also shown in Table 4 alongside the number-based results. The mass-based Φ_c estimates show the same trend as the number-based. However, the mass-based Φ_c determination is always higher than the number-based result. This is likely a ramification of the strong dependence of particle mass on particle diameter. Small particles have very little mass, so the initial increase in nucleation-mode particles does not increase the normalized mass as quickly as the normalized number of particles. This results in a slight shift of the mass-based Φ_c to slightly higher equivalence ratios.

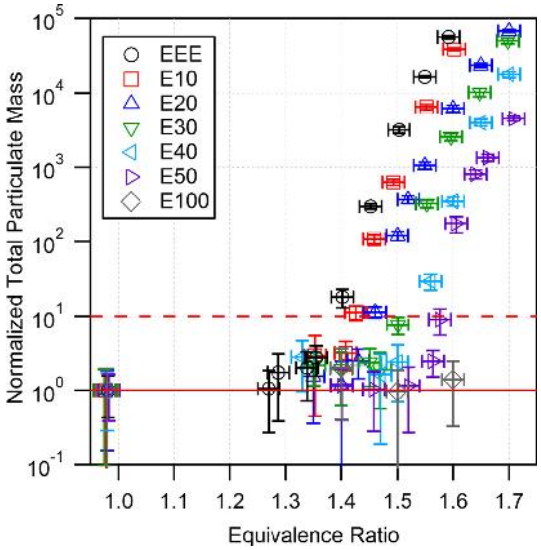

Fig. 10. Total particulate mass normalized to NFB shown with 10× threshold.

The mass-based and number-based critical equivalence ratios are plotted as a function of the ethanol vol.% in the fuel in Fig. 11. The results show a remarkable linear dependence of Φ_c on the ethanol vol.% in the fuel. Both curves were fit with lines of the form $\Phi_c = aV + b$, where V is the vol.% ethanol in the fuel. The coefficients for the curve fits are given in Table 5. The slopes for the mass-based and number-based curves are equal with mass-based results being consistently 0.03 higher. The results indicate that each% addition of ethanol to the fuel has the same effect of increasing the critical equivalence ratio by 0.004. Assuming that this linear trend continued up to 100% ethanol (100% denatured ethanol in the current case), the critical equivalence ratio would be 1.75 for E100 at the current engine conditions. This value is ~30% higher than the Φ_c for the baseline EEE gasoline. The results suggest, that from a chemistry standpoint, ethanol containing fuels always have a higher critical equivalence ratio for soot onset than the base gasoline fuel they are blended with. Therefore, increased particulate emissions observed in direct-injection engines for ethanol containing fuels are the result of fuel physical property impacts on mixture formation.

3.6. Comparison at constant Φ

To better visualize the change in particulate with ethanol blend percentage, Figs. 12 and 13 compare all fuels tested at constant

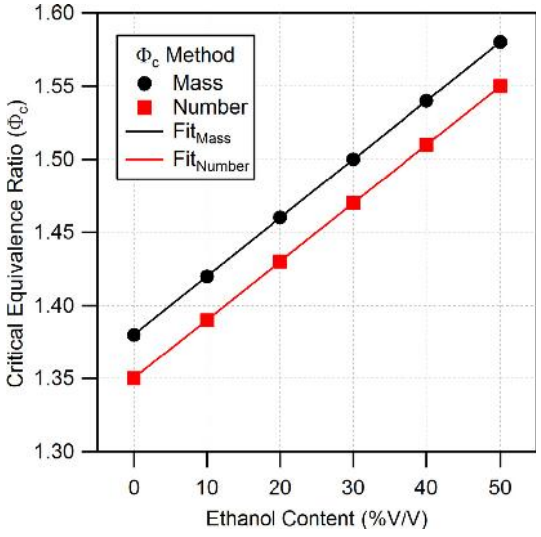

Fig. 11. Critical equivalence ratio for ethanol blends calculated using total number concentration and total mass concentration methods.

Table 5
Coefficients from linear fit of form $\Phi_c = aV + b$, where V is the vol.% ethanol, for the curve fits to the critical equivalence ratio versus ethanol vol.% data shown in Fig. 11.

	Mass	Number
a	0.004	0.004
b	1.38	1.35

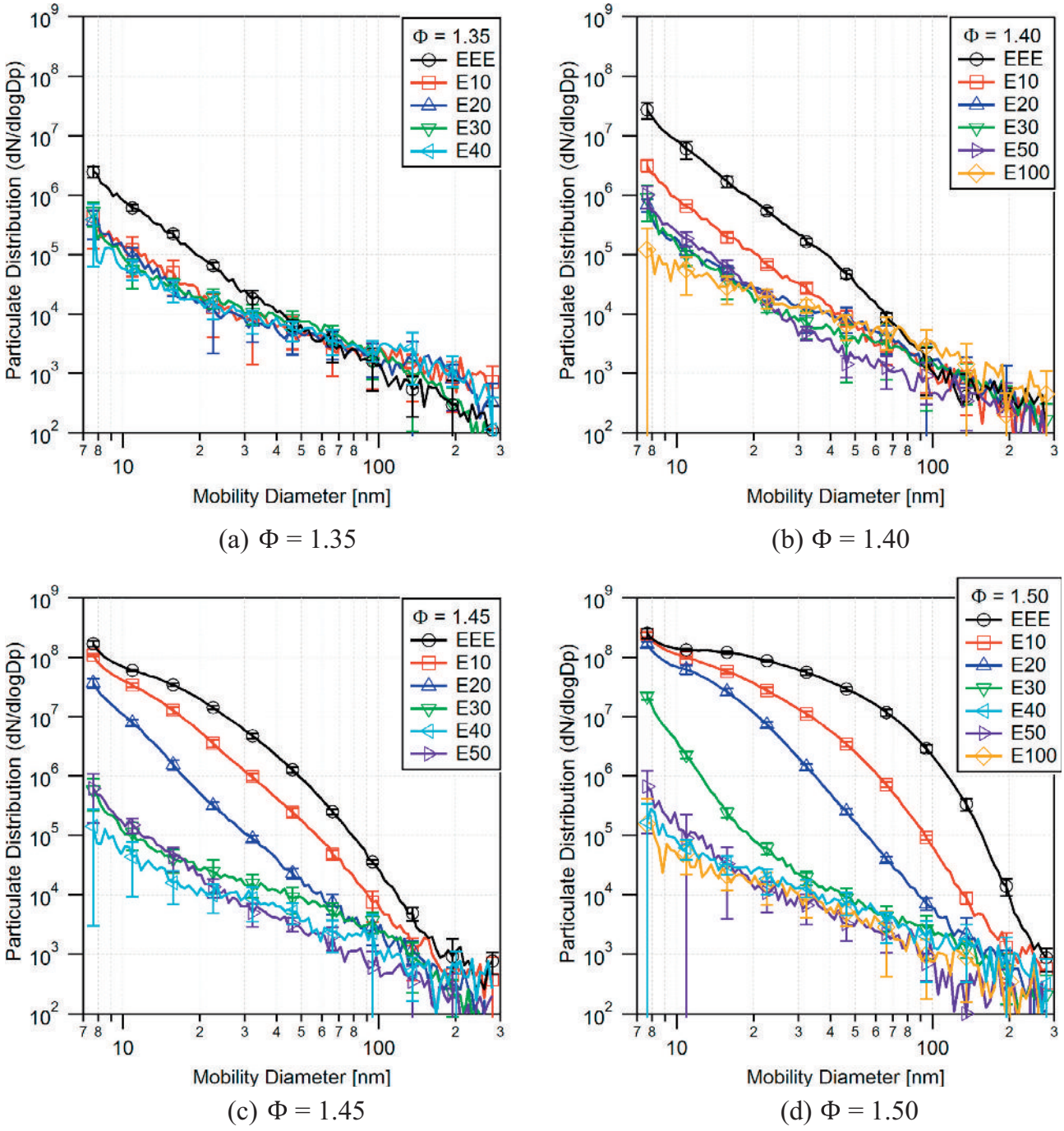

Fig. 12. Comparison of PSDs for ethanol-gasoline blends at equivalence ratios of 1.35–1.50.

equivalence ratios for Φ = 1.35–1.70. Beginning with Φ = 1.35 in Fig. 12(a), only EEE has begun to generate measurable particulate relative to the NFB. At each successive step in equivalence ratio, each fuel (in order of ethanol blend percentage) begins to rise above the NFB. Blends containing 40 and 50 vol.% ethanol are the last to reach their sooting threshold (of the blends tested, not including E100), both showing a sudden increase in the window 1.50 < Φ < 1.55. Visualizing the particulate data in this way also shows two additional trends: the consistent reduction in particulate and the shift in PSD shape with ethanol content. At each equivalence ratio, a clear reduction in particulate level can be seen with increasing ethanol for those PSDs which are above the NFB. This is especially well illustrated at Φ = 1.55/1.60 where all of the fuels are represented and a clear progression of particulate level with ethanol content can be seen.

Also visible at the high equivalence ratio is the shift from an accumulation-mode dominated distribution at lower ethanol blends to a nucleation-mode dominated PSD for higher ethanol blends. For fuels such as E40 and E50, the concentration of larger particles does not reach the level seen at lower ethanol blends at the equivalence ratios tested here. This trend is also seen when comparing the geometric mean mobility diameter for all of the conditions, shown in Fig. 14. The mean diameters for all of the fuels remain between 10 and 20 nm until a significant fraction of

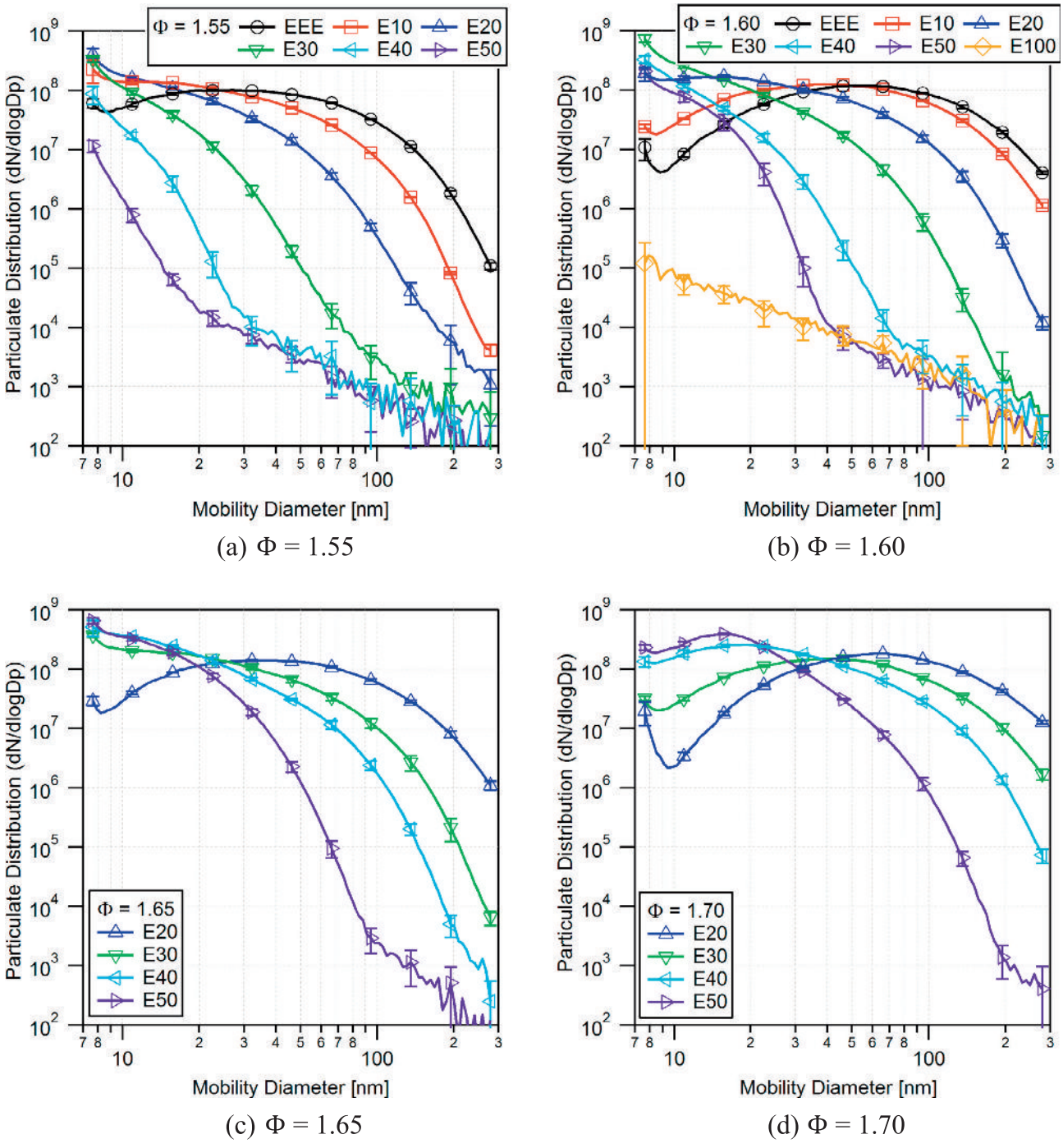

Fig. 13. Comparison of PSDs for ethanol-gasoline blends at equivalence ratios of 1.55–1.70.

agglomeration-mode particles appear which is followed by a reduction in nucleation-mode particles. This transition occurs when the mean diameter is approximately 30 nm and is indicated on the graph by the red dashed line. It can be seen that, for a given equivalence ratio, the mean diameter decreases significantly with ethanol addition. For higher ethanol blends such as E40 and E50, the mean diameter does not increase significantly, even at the highest equivalence ratios, due to the PSDs remaining nucleation-mode dominated. It is possible that increasing the equivalence ratio further would result in a similar steep increase in mean particle diameter once sufficiently high equivalence ratios are reached.

3.7. Comparison at constant C/O

Global equivalence ratio is the commonly used metric when comparing the sooting tendency of different engine running conditions. Generally, the higher the equivalence ratio is, the greater the sooting tendency. However, the equivalence ratio does not take into account the fuel-bound oxygen as the ratio moves away from stoichiometric. As a result, the total amount of oxygen available for oxidation is not truly considered. Conversely, the carbon-to-oxygen ratio provides a comparison of the number of carbon atoms in the mixture to the number of oxygen atoms available to oxidize the carbon. For non-oxygenated fuels, this compares the fuel

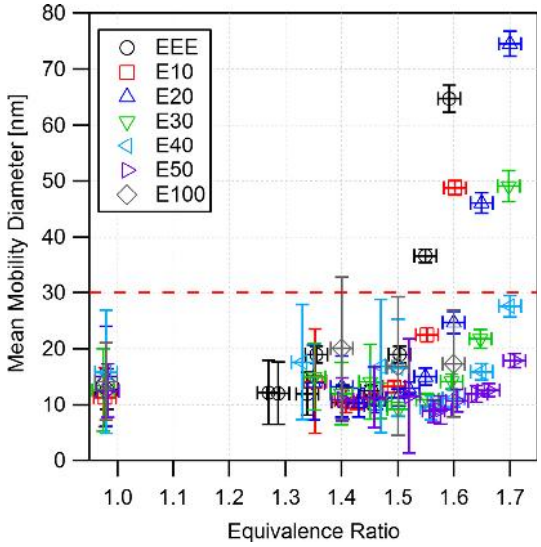

Fig. 14. Geometric mean mobility diameter of ethanol blends at all equivalence ratios.

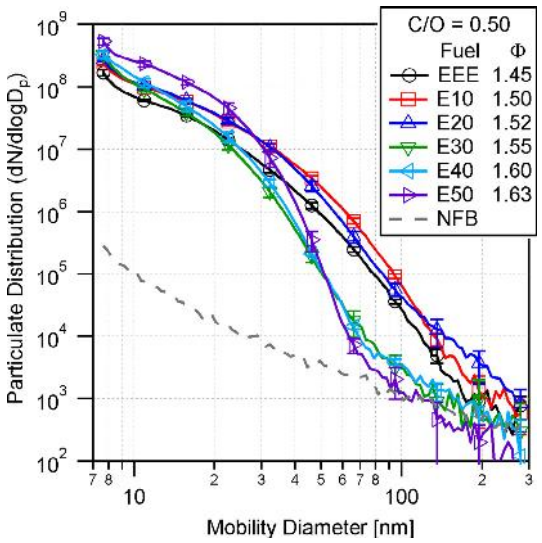

Fig. 16. Comparison of PSDs for EEE and ethanol-gasoline blends at C/O = 0.50.

carbon to oxidizer oxygen directly similar to equivalence ratio; however, for oxygenated fuels, the oxygen in the fuel is included to create a more representative metric. In previous sections it was shown that fuels with a higher ethanol percentage produced a much lower particle number despite having the same equivalence ratio. This may not fairly assess the relative influence of fuel bound oxygen and oxygen in the oxidizer (air), so the fuels were compared again on a constant C/O basis.

Two C/O ratios were chosen for comparison: 0.48 and 0.50. These were chosen such that each fuel would produce a sufficient level of particulate to make any effects readily apparent. The chosen C/O ratios also allows for all fuels, except E100, to be included. The corresponding equivalence ratios for E100 are near 2.0 for the C/O ratios of 0.48 and 0.5 which was too rich to achieve acceptable combustion stability. Comparisons at higher C/O ratios would have required prohibitively high equivalence ratios for the range of ethanol blends tested.

Figs. 15 and 16 show the comparisons of ethanol blends up to E50 for both C/O ratios. At both C/O ratios a distinct trend is seen where the behavior of the fuels can be separated into two groups: EEE-E20 and E30-E50. For C/O = 0.48, all of the fuels have a similar particle concentration at the smallest mobility diameter but the concentrations of lower-level ethanol blends decrease more slowly to NFB levels near 70 nm. On the other hand, higher ethanol concentrations decrease very quickly to the NFB, only showing significant particulate above the NFB for mobility diameters below 20 nm. At the higher C/O ratio of 0.50, the same dichotomy is present. EEE through E20 all have PSDs of similar shape and magnitude, with particulate levels above the NFB up to about 200 nm in diameter. Whereas, E30 to E50 all show a similar PSD shape with particulate levels more quickly falling to the NFB by 70 nm.

Noting a similar level of particulate for all of the fuels at similar C/O ratios, the normalized total number and mass results, previously shown versus equivalence ratio, were reexamined on a C/O ratio basis. These are shown in Figs. 17 and 18. As can be seen in the figures, converting to a C/O basis appears to collapse the data to a single curve. This occurs for both the number and mass-based comparisons. This indicates that, for a given C/O ratio, a similar level of particulate number or mass could be expected regardless of whether the oxygen was located in the fuel or oxidizer. While Figs. 15 and 16 show differences in the PSDs for

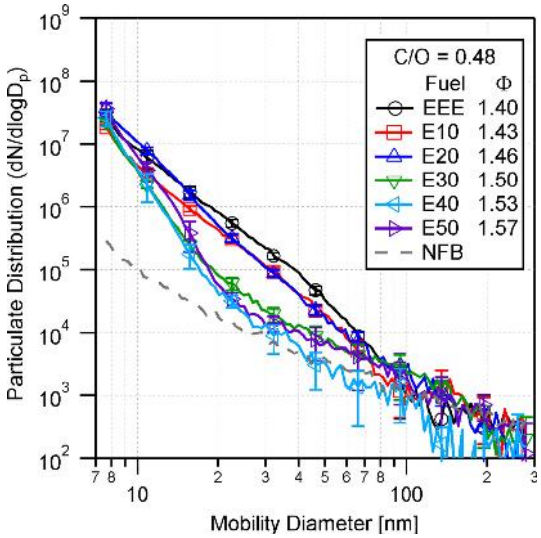

Fig. 15. Comparison of PSDs for EEE and ethanol-gasoline blends at C/O = 0.48.

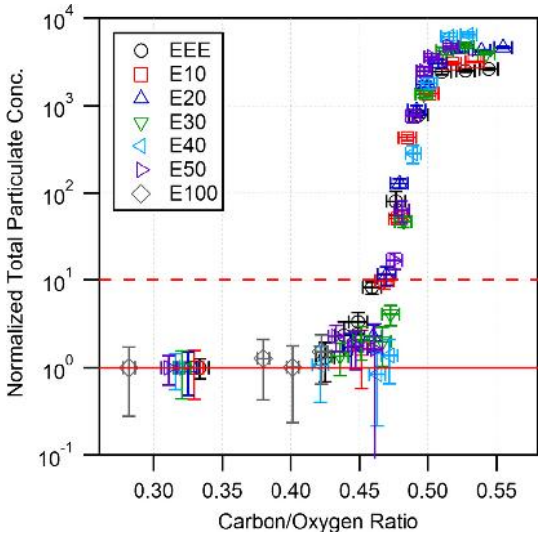

Fig. 17. Normalized total particulate concentration for all fuels vs. C/O ratio.

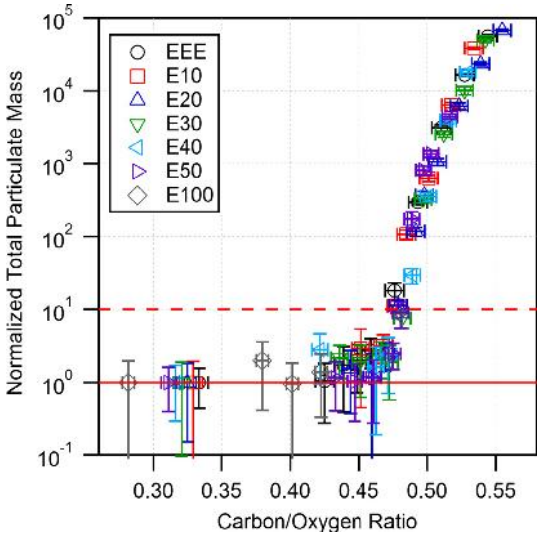

Fig. 18. Normalized total particulate mass for all fuels vs. C/O ratio.

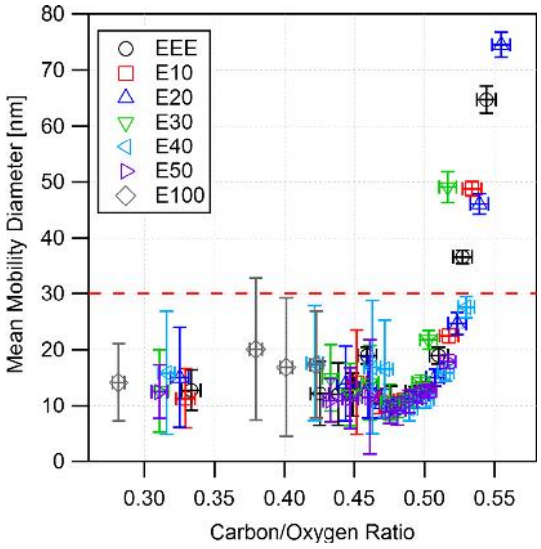

Fig. 19. Mean mobility diameter for all fuels vs. C/O ratio.

different amounts of ethanol, in the region with the highest number of particles the PSDs are similar in magnitude. These differences, while noticeable, are of sufficiently small magnitude such that the total number results are not significantly impacted. Figs. 17 and 18, while showing a definite general trend, are not able to completely capture the differences in PSD behavior between the different levels of ethanol blending.

Using a 10× NFB sooting threshold, just as was used to determine critical equivalence ratios for soot onset, the number and mass-based critical C/O ratios were found to be 0.463 ± 0.065 and 0.467 ± 0.041, respectively. Similarly, when the geometric mean mobility diameter is plotted versus C/O ratio for all of the fuels, shown in Fig. 19, the data collapses again. As was noted previously, when the mean mobility diameter exceeds ~30 nm, agglomerate particles will begin to dominate the PSD. Based on a linear regression, this threshold for agglomeration-mode occurs at C/O = 0.525 ± 0.072. It is important to note that, while all of the fuels reach the critical C/O threshold for both number and mass at approximately the same location, the mean diameter crosses the previously mentioned agglomeration-mode threshold much later.

4. Discussion

4.1. Matching of experimental conditions

In premixed flame studies, the addition of even small amounts of ethanol has been shown to decrease soot and soot precursors. The results of premixed combustion experiments in an IC engine in this study show similar trends. For ethanol combustion, the removal of carbon from the pathways which lead to soot production has been cited as one of the primary reasons for its reduced soot propensity. The CO bond in ethanol is strong enough under certain conditions to survive combustion and result in carbon monoxide formation, which does not lead to soot, potentially removing up to half of the carbon in ethanol from soot forming pathways [4,30].

Sooting propensity is strongly temperature dependent and temperatures need to be matched to make direct comparisons of sooting tendency. For the current work, the change in temperature over the equivalence ratio range where the sooting threshold is crossed is very small. Additionally, at matched equivalence ratio, or matched C/O ratio, the changes are relatively small between fuels, less than ~100 K. To confirm this, the in-cylinder temperature (determined using a single-zone ideal gas calculation) for each case was averaged over the time spent in the temperature range where 1900 K > T > 1350 K and the results are plotted in Fig. 20(a). This temperature range was chosen as it corresponds to the range of temperatures where soot formation is most likely and occurs at the highest rate in premixed flames [27,31,32]. The time over which the temperature was in this range was also determined and is plotted in Fig. 20(b). Aside from the stoichiometric cases, which are far from the sooting threshold, the average temperature for all cases are within 30 K of each other. At a given equivalence ratio, the difference in average temperatures is <20 K. Furthermore, the time duration in the critical soot formation temperature range of 1350 K < T < 1900 K, where soot onset is most likely and the production of soot is fastest, is similar (within about 1.5 ms at a given equivalence ratio) for all of the fuels tested. Although the pressure may be slightly different for a given temperature, the pressure effect is thought to be closer to linear and less than the temperature dependence which is exponential [31].

4.2. Effect of fuel-bound oxygen

The addition of ethanol to gasoline in this study results in steady decrease in soot production as demonstrated by the linear increase in critical equivalence ratio. A similar trend was also seen when ethanol was added to gasoline turbulent spray flames [13]. It has been argued in the literature that the reduction in soot formation with ethanol addition is due to dilution, or the replacement of a more sooting fuel with less sooting ethanol [16,30]. However, work done by Kasper et al., Lemaire and coworkers, and Pepiot-Desjardins et al. have shown that the dilution effect of ethanol is only partly responsible for soot reduction and that the fuel-bound oxygen also plays a role, where the effectiveness of the oxygen is determined by both the oxygenate and base fuel [13,33,34].

To further examine the effect of the fuel-bound oxygen, we can make the assumption that the carbon which is already bound to an oxygen is removed from the soot formation pathway. This would leave only the unbound carbon available to form soot. Let C_β and O_{air} be the moles of unbounded fuel carbon injected per cycle and moles of oxygen in air per cycle, respectively. The C/O ratio can now be expressed in terms of C_β and O_{air} to determine if oxygen-bound carbon is being used to form soot. As can be seen in Fig. 21, for a similar C_β/O_{air} ratio, ethanol

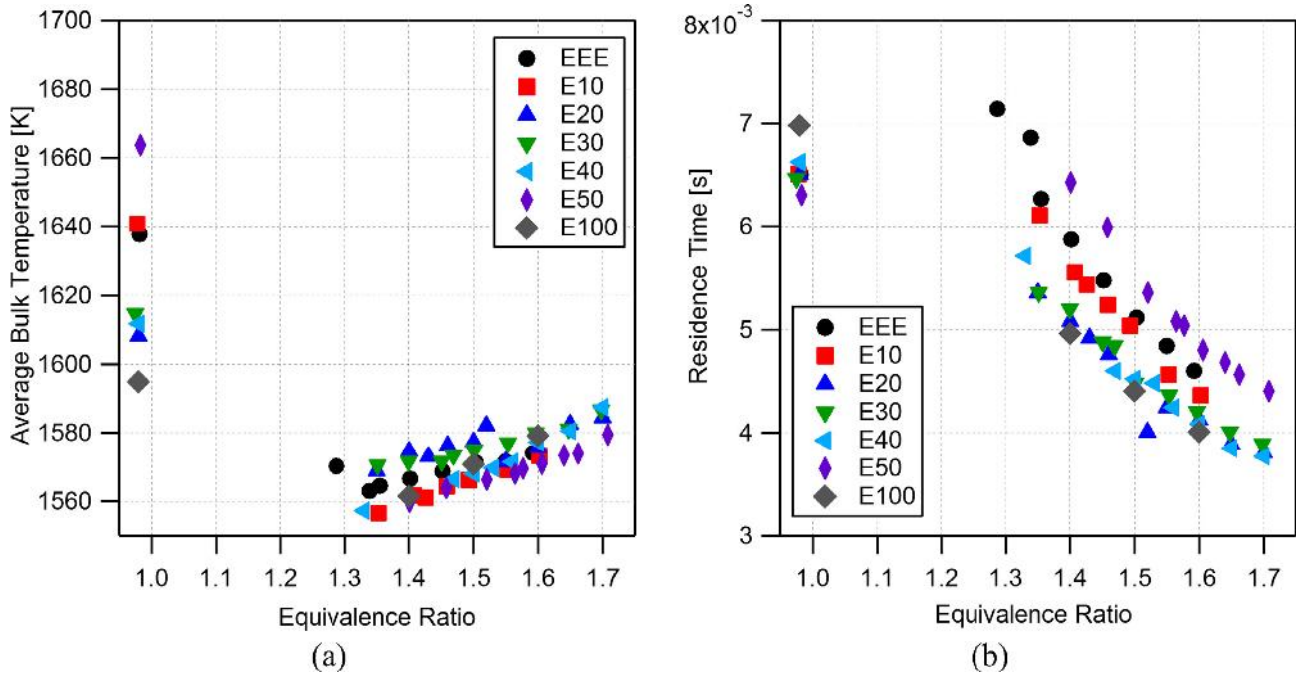

Fig. 20. Average temperature (a) and residence time (b) in critical sooting temperature range of 1350 K < T < 1900 K.

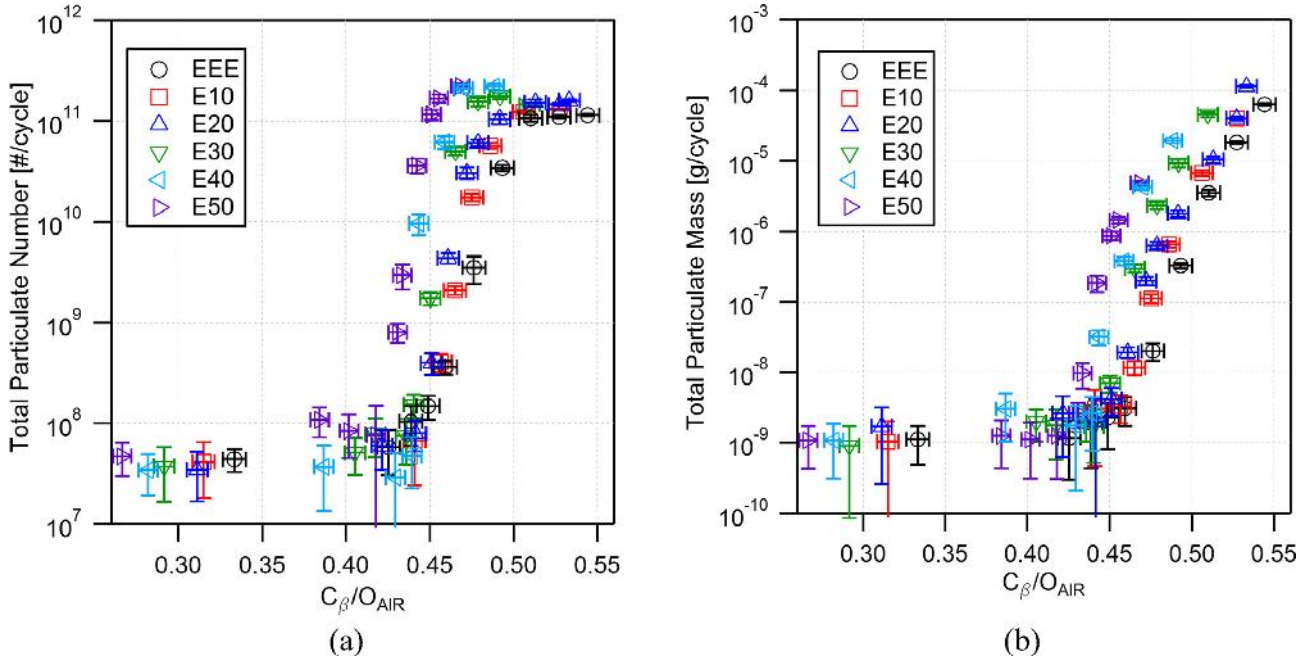

Fig. 21. Total particulate number (a) and total particulate mass (b) shown against modified C/O ratio, C_β/O_{air}, where C_β is the moles of unbounded fuel carbon injected per cycle and O_{air} and moles of oxygen in air per cycle.

blends produce higher particulate number and mass. In fact, increasing ethanol content results in further increases in number and mass. This indicates that oxygen-bound carbon is indeed participating in soot formation pathways though it is difficult to quantify to what extent. It was previously shown that comparing the results against a global C/O ratio was able to collapse the data into singular curves, despite ethanol having at least some carbon which does not participate in soot formation. This could indicate that the soot-reducing effect of the oxygen-bound carbon is not very substantial.

4.3. Carbon/oxygen ratio

Since equivalence ratio only compares the air-fuel mixture to that of its stoichiometric counterpart with no consideration for fuel-bound oxygen, it seems unable to adequately represent the mixture's actual stoichiometry. Conversely, the carbon-oxygen ratio of the air-fuel mixture takes into account all of the carbon and oxygen in the mixture. This metric has also been widely used in the literature over the years to describe the sooting tendency of fuels [35,36]. The results in this work further support that C/O ratio

is an appropriate method to characterize the sooting tendency of fuel-oxidizer mixtures, including oxygenated fuels, such as gasoline-ethanol blends. C/O ratio appears to be a controlling parameter for overall particle concentration, overall particle mass, and mean mobility diameter, the latter of which can be used to infer the characteristics of the PSD.

The results shown here suggest that having an equal amount of carbon to oxygen between these air-fuel mixtures will produce similar amounts of particulate; however, differences in the particulate size distributions, with respect to ethanol content, are still visible. As was seen in the C/O results, there was a distinct change in PSD shape once the ethanol content reached 30%. For C/O = 0.48, this resulted in only particles with $d_m < 20$ nm being produced at ethanol concentrations greater than 30%. At C/O = 0.50, similar levels of nucleation-mode particles were produced for all fuels but blends with more than 30% ethanol by volume produced almost no large agglomerates. Similar results were seen by Salamanca et al. in ethylene premixed flames where ethanol addition appeared to reduce soot coagulation efficiency, reducing larger diameter particulate while still having high numbers of nanoparticles [2,8]. Lemaire et al. also found that soot formed by gasoline-ethanol blends oxidized faster, further reducing overall soot production [13]. This effect would appear small at lower ethanol blends but become more prominent as the overall carbon number in the fuel mixture decreases. In simulations with n-heptane mixed with oxygenates, including methanol, ethanol, dimethoxy methane, and dimethyl ether, Curran predicted that soot precursors could be reduced to negligible levels when the oxygen weight percentage in the fuel reached 30%, regardless of which oxygenate was used [30]. This was confirmed in experiments done by Miyamoto and coworkers [37]. For ethanol-gasoline mixtures, this percentage does not reach 30% until ethanol content reaches ~85% by volume; however, it is evident based on the results shown here that there is measurable soot reduction for even E20 blends, which contain just under 8% oxygen by weight.

5. Conclusions

In this work, the relative sooting propensity of different ethanol blends under completely premixed and prevaporized operation was investigated. By operating the engine in this mode, the presence of liquid fuel in-cylinder was eliminated allowing the examination of soot production from gas phase sources. The results shown here build upon premixed flame studies in the literature and examine soot production from premixed combustion of ethanol-gasoline fuels in an IC engine. To the authors' knowledge, this is the first study which examines the effect of ethanol on particulate formation in an IC engine over such a wide range of ethanol-gasoline blends while removing the physical effects of the fuel itself. This has allowed the examination of the chemical effect of the fuel on particulate formation. The equivalence ratio at soot onset, Φ_c, was shown to increase with ethanol content. The results also show that, for the same equivalence ratio, increasing the fraction of ethanol in the fuel will reduce particulate levels in the engine exhaust. This result supports what has been seen in the literature for premixed flame studies. As ethanol content increases, the PSD changes from agglomeration- to nucleation-mode dominated size distributions. At higher equivalence ratios, this shift also corresponds to the change from an accumulation-mode dominated distribution for low level ethanol blends to a nucleation-mode dominated distribution at higher blends. Additionally, global C/O ratio appears to collapse the sooting propensity of all ethanol blends. Blends at equivalence ratios which have a similar C/O ratio produce similar levels of particulate, although the size distributions can be noticeably different depending on the ethanol content. These results imply that higher levels of particulate formation from typical DI combustion are attributable to pockets of significantly higher equivalence ratios, possibly diffusion-limited combustion, which can arise from liquid fuel sources. This is especially true when ethanol makes up a significant volume fraction of the fuel. In the future, the results shown here may be used to make more informed hypotheses regarding in-cylinder particulate formation under direct-injection operation.

Acknowledgements

This work was funded by the DOE Great Lakes Bioenergy Research Center (DOE BER Office of Science DE-FC02-07ER64494).

References

[1] EPA. Ethanol Waivers (E15 and E10). Environmental Protection Agency; 2011.
[2] Salamanca M, Sirignano M, D'Anna A. Particulate formation in premixed and counter-flow diffusion ethylene/ethanol flames. Energy Fuels 2012;26:6144–52.
[3] Hoon Song K, Nag P, Litzinger TA, Haworth DC. Effects of oxygenated additives on aromatic species in fuel-rich, premixed ethane combustion: a modeling study. Combust Flame 2003;135:341–9.
[4] Wu J, Song KH, Litzinger T, Lee S-Y, Santoro R, Linevsky M, et al. Reduction of PAH and soot in premixed ethylene–air flames by addition of ethanol. Combust Flame 2006;144:675–87.
[5] Yakimov S, Knyaz'kov D, Bol'shova T, Shmakov A, Korobeinichev O, Qi F. Investigation of the effect of ethanol additives on the structure of low-pressure ethylene flames by photoionization mass spectrometry. Combust Explo Shock Waves 2012;48:609–19.
[6] McEnally CS, Pfefferle LD. The effects of dimethyl ether and ethanol on benzene and soot formation in ethylene nonpremixed flames. Proc Combust Inst 2007;31:603–10.
[7] McNesby KL, Miziolek AW, Nguyen T, Delucia FC, Skaggs RR, Litzinger TA. Experimental and computational studies of oxidizer and fuel side addition of ethanol to opposed flow air/ethylene flames. Combust Flame 2005;142:413–27.
[8] Salamanca M, Sirignano M, Commodo M, Minutolo P, D'Anna A. The effect of ethanol on the particle size distributions in ethylene premixed flames. Exp Thermal Fluid Sci 2012;43:71–5.
[9] Rubino L, Thomson MJ. The effect of oxygenated additives on soot precursor formation in a counterflow diffusion flame. SAE Technical Paper; 1999.
[10] Alexiou A, Williams A. Soot formation in shock-tube pyrolysis of toluene, toluene-methanol, toluene-ethanol, and toluene-oxygen mixtures. Combust Flame 1996;104:51–65.
[11] Frenzel I, Trimis D. Study on the influence of ethanol addition on exhaust gas composition and soot formation in iso-octane flames. Proceedings of the European Combustion Meeting; 2015.
[12] Inal F, Senkan SM. Effects of oxygenate additives on polycyclic aromatic hydrocarbons (PAHs) and soot formation. Combust Sci Technol 2002;174:1–19.
[13] Lemaire R, Therssen E, Desgroux P. Effect of ethanol addition in gasoline and gasoline–surrogate on soot formation in turbulent spray flames. Fuel 2010;89:3952–9.
[14] Maricq MM. Soot formation in ethanol/gasoline fuel blend diffusion flames. Combust Flame 2012.
[15] Golea D, Rezgui Y, Guemini M, Hamdane S. Reduction of PAH and soot precursors in benzene flames by addition of ethanol. J Phys Chem A 2012;116:3625–42.
[16] Liu D. Detailed influences of ethanol as fuel additive on combustion chemistry of premixed fuel-rich ethylene flames. Sci China Technol Sci 2015;58:1696–704.
[17] Kohse-Höinghaus K, Oßwald P, Struckmeier U, Kasper T, Hansen N, Taatjes CA, et al. The influence of ethanol addition on premixed fuel-rich propene–oxygen–argon flames. Proc Combust Inst 2007;31:1119–27.
[18] Butler AD, Sobotowski RA, Hoffman GJ, Machiele P. Influence of fuel PM Index and ethanol content on particulate emissions from light-duty gasoline vehicles. SAE Technical Paper; 2015.
[19] He X, Ireland JC, Zigler BT, Ratcliff MA, Knoll KE, Alleman TL, et al. The impacts of mid-level biofuel content in gasoline on SIDI engine-out and tailpipe particulate matter emissions. SAE Technical Paper; 2010.
[20] Storey JM, Barone TL, Thomas JF, Huff SP. Exhaust particle characterization for lean and stoichiometric DI vehicles operating on ethanol-gasoline blends. SAE Technical Paper; 2012.
[21] Price P, Twiney B, Stone R, Kar K, Walmsley H. Particulate and hydrocarbon emissions from a spray guided direct injection spark ignition engine with oxygenate fuel blends; 2007
[22] Dutcher DD, Stolzenburg MR, Thompson SL, Medrano JM, Gross DS, Kittelson DB, et al. Emissions from ethanol-gasoline blends: a single particle perspective. Atmosphere 2011;2:182–200.

[23] Karavalakis G, Short D, Russell RL, Jung H, Johnson KC, Asa-Awuku A, et al. Assessing the impacts of ethanol and isobutanol on gaseous and particulate emissions from flexible fuel vehicles. Environ Sci Technol 2014;48:14016–24.
[24] Szybist JP, Youngquist AD, Barone TL, Storey JM, Moore WR, Foster M, et al. Ethanol blends and engine operating strategy effects on light-duty spark-ignition engine particle emissions. Energy Fuels 2011;25:4977–85.
[25] Catapano F, Di Iorio S, Lazzaro M, Sementa P, Vaglieco B. Effect of ethanol blends on soot formation and emissions in a GDI optical engine. Meeting of the Italian Section of the Combustion Institute; 2013.
[26] Di Iorio S, Lazzaro M, Sementa P, Vaglieco BM, Catapano F. Particle size distributions from a DI high performance si engine fuelled with gasoline-ethanol blended fuels. SAE Technical Paper; 2011.
[27] Hageman MD, Sakai SS, Rothamer DA. Determination of soot onset and background particulate levels in a spark-ignition engine. Proc. Combust. Inst. 2014.
[28] Zelenyuk A, Reitz P, Stewart M, Imre D, Loeper P, Adams C, et al. Detailed characterization of particulates emitted by pre-commercial single-cylinder gasoline compression ignition engine. Combust Flame 2014;161:2151–64.
[29] Viswanathan S, Rothamer DA, Foster DE, Fansler TD, Zelenyuk A, Stewart ML, et al. Evolution of deep-bed filtration of engine exhaust particulates with trapped mass. Int J Engine Res 2016;1468087416675094.
[30] Curran HJ, Fisher EM, Glaude P-A, Marinov NM, Pitz W, Westbrook C, et al. Detailed chemical kinetic modeling of diesel combustion with oxygenated fuels. SAE Technical Paper; 2001.
[31] Böhm H, Hesse D, Jander H, Lüers B, Pietscher J, Wagner H, et al. The influence of pressure and temperature on soot formation in premixed flames. In: Symposium (international) on combustion. Elsevier; 1989. p. 403–11.
[32] Glassman I. Soot formation in combustion processes. Symp (Int) Combust 1989;22:295–311.
[33] Kasper TS, Oßwald P, Kamphus M, Kohse-Höinghaus K. Ethanol flame structure investigated by molecular beam mass spectrometry. Combust Flame 2007;150:220–31.
[34] Pepiot-Desjardins P, Pitsch H, Malhotra R, Kirby SR, Boehman AL. Structural group analysis for soot reduction tendency of oxygenated fuels. Combust Flame 2008;154:191–205.
[35] Haynes B, Jander H, Wagner HG. Optical studies of soot-formation processes in premixed flames. Ber Bunsenges Phys Chem 1980;84:585–92.
[36] Millikan RC. Non-equilibrium soot formation in premixed flames. J Phys Chem 1962;66:794–9.
[37] Miyamoto N, Ogawa H, Nabi M. Approaches to extremely low emissions and efficient diesel combustion with oxygenated fuels. Int J Engine Res 2000;1:71–85.